A look-up table method based on unstructured grids and its application to non-ideal compressible fluid dynamic simulations

Rubino, A.; Pini, M.; Kosec, M.; Vitale, S.; Colonna, P.

DOI
10.1016/j.jocs.2018.08.001

Publication date
2018

Document Version
Final published version

Published in
Journal of Computational Science

Citation (APA)
Rubino, A., Pini, M., Kosec, M., Vitale, S., & Colonna, P. (2018). A look-up table method based on unstructured grids and its application to non-ideal compressible fluid dynamic simulations. *Journal of Computational Science*, *28*, 70-77. https://doi.org/10.1016/j.jocs.2018.08.001

Journal of Computational Science 28 (2018) 70–77

Contents lists available at ScienceDirect

Journal of Computational Science

journal homepage: www.elsevier.com/locate/jocs

A look-up table method based on unstructured grids and its application to non-ideal compressible fluid dynamic simulations

A. Rubino [a], M. Pini [a,*], M. Kosec [b], S. Vitale [a], P. Colonna [a]

[a] Delft University of Technology, Aerospace Engineering Faculty, Propulsion and Power, Kluyverweg 1, 2629 HS Delft, The Netherlands
[b] Stanford University, Aeronautics and Astronautics, Stanford, 94305 CA, United States

ARTICLE INFO

Article history:
Received 28 May 2018
Received in revised form 18 July 2018
Accepted 1 August 2018
Available online 9 August 2018

Keywords:
Look-up table
Trapezoidal map
Unstructured mesh
Thermodynamic modeling
Interpolation
Real-gas flows
Non-ideal compressible flow
NICFD
CFD

ABSTRACT

Fast and accurate computation of thermo-physical properties is essential in computationally expensive simulations involving fluid flows that significantly depart from the ideal gas or ideal liquid behavior. A look-up table algorithm based on unstructured grids is proposed and applied to non-ideal compressible fluid dynamics simulations. The algorithm grants the possibility of a fully automated generation of the tabulated thermodynamic region for any boundary and to use mesh refinement. Results show that the proposed algorithm leads to a computational cost reduction up to one order of magnitude, while retaining the same accuracy level compared to simulations based on more complex equation of state. Furthermore, a comparison of the LuT algorithm with a uniformly spaced quadrilateral tabulation method resulted in similar performance and accuracy.

1. Introduction

The accurate estimation of thermo-physical properties of fluids is essential for many engineering and scientific applications, and it requires complex models in case the behavior of the fluid departs from that of the ideal gas or ideal liquid. Fluids exhibiting non-ideal behavior are involved in various technologies such as advanced power and propulsion systems, refrigeration and air conditioning systems, oil and gas processes, etc. [1–4]. In these cases, the evaluation of thermo-physical properties is often necessary for system design and performance evaluation or to simulate the flow behavior within components. Fluid dynamic simulations of vapors in non-ideal states are also employed in more fundamental research (see, e.g., Ref. [5]) and the branch of fluid mechanics dealing with this type of fluid flows was recently termed *non-ideal compressible fluid dynamics* (NICFD) [6].

The computational cost associated with fluid thermodynamic models expressed in terms of equations of state (EoS) can become a limiting factor if accurate estimations are needed in combination with expensive simulations. This is the case, e.g., in the design and optimization of industrial components [7] or in computational fluid dynamics (CFD) [8]. In order to decrease the computational time related to the calculation of thermo-physical fluid properties, while maintaining a satisfactory level of accuracy, look-up table (LuT) methods are convenient and widely adopted [9].

A LuT method consists of three basic parts: 1. The tabulation of a discrete set of values of thermodynamic properties pertaining to states generated with a given EoS-base model; 2. A search algorithm; 3. An interpolation method. Since the tabulation is performed only once, at preprocessing level, this way of evaluating fluid thermophysical properties can greatly reduce the computational effort if the models are based on complex EoS, provided that the associated search algorithm is efficient. Furthermore, the interpolation technique must be carefully chosen in order to achieve a satisfactory level of accuracy, which is a fundamental requirement to guarantee convergence in CFD simulations and accuracy of the final result. LuT methods based on a structured mesh of thermodynamic region of interest have been documented in the literature [10,11,9,12]. In order to increase the accuracy and decreasing the number of discretization points for thermodynamic region of interest, algorithms based on adaptive Cartesian mesh have been proposed [13,14]. However, the use of quadrilateral grids, in combination with local refinement, can lead to local discontinuities and poor interpolation accuracy of properties in the proximity of smooth boundaries [15,13]. This can especially occur for proper-

* Corresponding author.
E-mail address: M.Pini@tudelft.nl (M. Pini).

https://doi.org/10.1016/j.jocs.2018.08.001

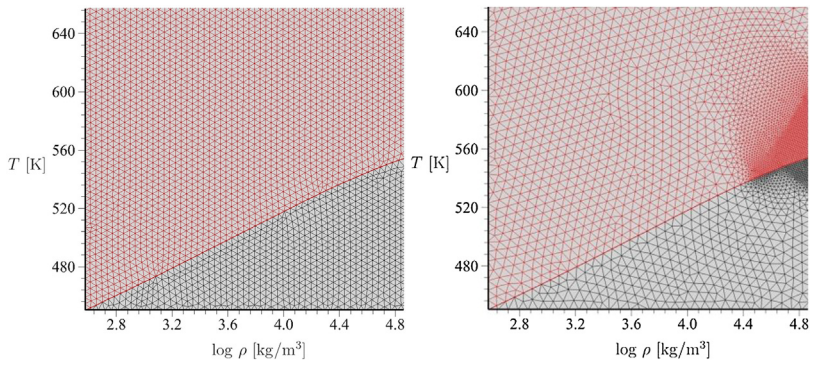

(a) Thermodynamic mesh. (b) Thermodynamic mesh refined.

Fig. 1. Thermodynamic triangular mesh for the siloxane MDM. (a) Regular thermodynamic mesh. (b) Refined thermodynamic mesh.

ties reconstruction or for interpolation close to the vapor–liquid saturation line.

The study described here resulted in *ug-LUT*, a new LuT method based on meshing thermodynamic region of interest by means of unstructured triangular grids. The generation of multidimensional thermodynamic tables is fully automated, even in case multiple fluid phases need to be computed. Unstructured grids allow for mesh refinements, a valuable feature in case of strong property variations, which occur in proximity of the vapor–liquid critical point, and of the saturation line in general. The *ug-LUT* method is applicable also to multi-component fluids. A search algorithm based on a trapezoidal map of the tabulated region contributes significantly to its computational efficiency. The *ug-LUT* method for thermo-physical property calculations is implemented within the open-source code *SU2* [16–18] and its verification is presented by means of paradigmatic CFD test cases of increasing fidelity. Finally, the *ug-LUT* algorithm is compared to a structured-based LuT with the aim of assessing its computational cost and memory requirements.

2. Method

2.1. Generation of thermodynamic mesh

An unstructured mesh is generated for thermodynamic domain of interest. A 2D grid generator [19], based on the Advancing-Delaunay front method, is used in this study. The adopted grid generator allows for local refinements in selected regions of thermodynamic domain. Fig. 1 shows examples of thermodynamic meshes for siloxane MDM (octamethyltrisiloxane, $C_8H_{24}O_2Si_3$), generated by selecting T and $\log(\rho)$ as input state variables. The use of unstructured mesh in combination with local refinement is proposed here as an effective alternative to structured and quad-tree grids. Quad-tree based algorithms are efficient for controlling the mesh refinement level, but can suffer from the following issues [15,13]: (i) storing and retrieving the mesh connectivity associated to the recursive tree structure; (ii) hanging nodes at different sizes cells interfaces, if continuous property reconstruction is required; (iii) additional interpolation, triangulation or a curvilinear mesh system might be necessary to reconstruct smooth boundaries (e.g. vapor–liquid saturation line).

Once the mesh patches are generated using any suitable set of state variables (two if the fluid is pure), all other needed fluid thermo-physical properties are computed at each mesh node with an appropriate thermodynamic library. The current implementation of the *ug-LUT* method makes use of an external thermodynamic library [20], which embeds a large variety of models based on complex equations of state (EoS). As an example, Fig. 2 reports the

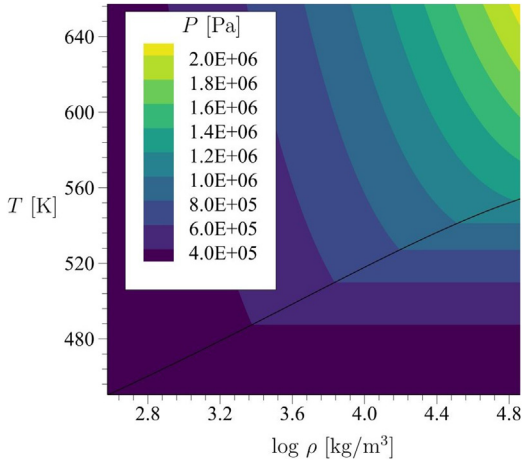

Fig. 2. Tabulated pressure contours obtained for the siloxane MDM.

pressure contour for siloxane MDM, obtained using a model based on an EoS in the *Span-Wagner* functional form [21].

2.2. Search algorithm

Once the set of thermo-physical properties for the selected fluid are stored in tabular form, a search algorithm is used to retrieve the best approximation of the query state or point. A point location algorithm based on a trapezoidal map has been adopted [22] because of the following considerations: (i) the same geometrical connectivity is used for all the search pairs. This is especially beneficial because the connectivity has not to be recomputed for each search pair and it can be used to search in highly skewed thermodynamic planes. As an example for this, if the initial thermodynamic mesh is built for the (P, ρ) plane, the resulting mesh on the (h, s) plane will be highly skewed; (ii) searching for the triangle containing the query vector by resorting to algorithms that do not use the mesh connectivity information (e.g. *kd-tree*) on an irregular and highly skewed grid can lead to inaccurate interpolation; (iii) trapezoidal maps work for general polyhedra. The search algorithm can be used to switch between different mesh zones, characterized by a polyhedron outline. This feature allows to avoid a mapping for grids not conforming with a rectangular thermodynamic domain [13].

Given the set S of n triangular mesh edges, the trapezoidal map $T(S)$ is built according to the following steps (see Fig. 3):

1. a unique set of edges and the corresponding list of its x coordinates is created by filtering out duplicates;

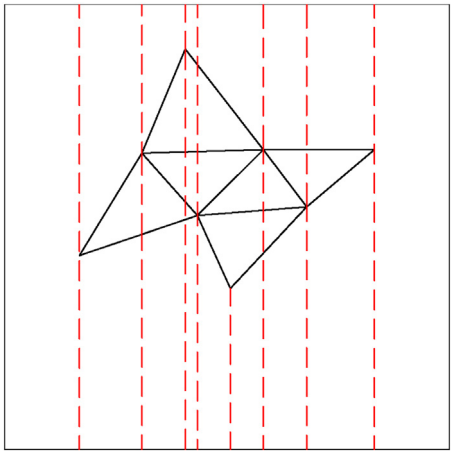

Fig. 3. Schematic representation of the trapezoidal map for an unstructured grid.

2. the intersecting edges are associated to each band;
3. the edges in each band are sorted.

The trapezoidal map $T(S)$ is created in a preprocessing stage for each thermodynamic search pair, e.g., (h, s), (ρ, v), etc. A more detailed description of the trapezoidal map algorithm can be found in Appendix A.

The mesh simplex, containing the query point q within $T(S)$, is identified according to the following procedure:

1. the x coordinate of the query point is obtained with a binary search for its containing band;
2. within the containing band, the edge above and the one below the query point are identified;
3. the simplex containing the query point is singled out by using the edge-to-face connectivity of the two edges selected during the previous step.

The query algorithm is also detailed in Appendix A.

2.3. Interpolation method

A two-dimensional linear interpolation problem can be written as

$$f(x, y) = \Sigma_{i=1}^{N} w_i g_i(x, y) = W^T G(x, y) = G^T(x, y) W, \tag{1}$$

where $G(x, y)$ is an interpolation basis which transforms the query coordinates x, y (raw features) into N linearly independent interpolation features. An example of a polynomial basis function $G(x, y)$ on a triangle (three points, $N = 3$) is given by

$$G(x, y) = [1, x, y]^T. \tag{2}$$

In the implemented thermodynamic look-up-table, the two-dimensional coordinates are thermodynamic pairs such as (ρ, u), (P, T), (h, s). This choice of $G(x, y)$ was found to be sufficiently accurate, provided that a relatively fine mesh for the look-up-table is used. The vector of weights W is found through

$$A = \begin{bmatrix} G^T(x_1, y_1) \\ \vdots \\ G^T(x_i, y_i) \\ \vdots \\ G^T(x_N, y_N) \end{bmatrix}, \qquad F = \begin{bmatrix} f(x_1, y_1) \\ \vdots \\ f(x_i, y_i) \\ \vdots \\ f(x_N, y_N) \end{bmatrix}, \qquad AW = F \tag{3}$$

where N is the number of sample points on which the interpolation is based and the $f(x_i, y_i)$ are the known values. F is an implicit function of the query point (x_q, y_q). The mapping from the query point to the forcing vector F is given by the trapezoidal map algorithm, which provides the interpolation points. The interpolation is computationally efficient when a single function is being interpolated at many different combinations of query point coordinates (x_q, y_q), as all the sample points can use the same weights.

However, the completion of thermodynamic look-up-table requires the interpolation of several functions (ten or more) for each query point. Thus, it is convenient to work out the dual form of the primal interpolation problem, such that the weights have to be computed only once for a given query point. The dual problem can be written as

$$G(x_q, y_q)^T W = F^T V, \tag{4}$$

where the interpolation weights V are now the adjoint solution of

$$A^T V = G(x_q, y_q). \tag{5}$$

The equivalence of the two formulations can be put into evidence by [23]

$$V^T F = V^T (AW) = (A^T V)^T W = G(x_q, y_q)^T W. \tag{6}$$

The weights V can be computed once for a given query point and reused to calculate the different thermodynamic properties of interest. For example, if twelve properties need to be interpolated, only one matrix-multiplication is required per each mesh triangle, instead of the twelve which would be needed with the primal interpolation method. Additionally, since the $(A^T)^{-1}$ matrix depends only on a priori established values, it can be completely pre-computed without additional runtime cost. If the condition number of the matrix is high, a pseudo-inverse should be applied; in this case pre-computation is only possible with the primal interpolation.

3. Application to NICFD simulations

In order to verify and provide information on the performance of the *ug-LUT* method, three CFD test cases of increasing complexity level are discussed. The selected test cases feature expansions characterized by relevant non-ideal compressible flow effects, requiring the use of complex equations of state to accurately compute the flow behavior. The simulations are performed with *SU2* [16], a code previously verified for non-ideal compressible fluid dynamics simulations [24]. For all test cases, the convective fluxes are discretized by a generalized Roe scheme [25,24], and second-order accuracy is achieved with the *MUSCL* approach [26]. Ref. [16] provides a more detailed description of the flow solver and the associated numerical methods.

Thermodynamic properties needed by the flow solver, whose value is interpolated from the values stored in the LuT, are

$$\rho, P, T, c, e, h, s, \left(\frac{\partial P}{\partial \rho}\right)_e, \left(\frac{\partial P}{\partial e}\right)_\rho.$$

The partial derivatives of the pressure are necessary to calculate the convective fluxes in non-ideal compressible flow simulations, see, e.g., Ref. [18].

3.1. 2D supersonic nozzle

The geometry of the converging–diverging supersonic nozzle is depicted in Fig. 5a, together with the Mach contour resulting from the Euler simulation. The two-dimensional flow domain is discretized with approximately 15,000 triangular mesh elements

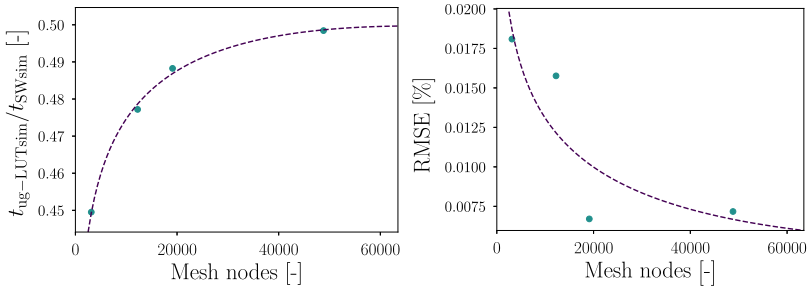

(a) Normalized computational cost. (b) RMSE error.

Fig. 4. 2D inviscid supersonic nozzle simulation results. (a) Normalized computational cost of the simulation employing the look-up table method (*ug-LUTsim*) compared to that of the simulation obtained using the Span-Wagner thermodynamic model (*SWsim*). (b) Relative mean square error (RMSE) of the Mach field from the *SWsim* and *ug-LUTsim*. The *SWsim* results are taken as reference.

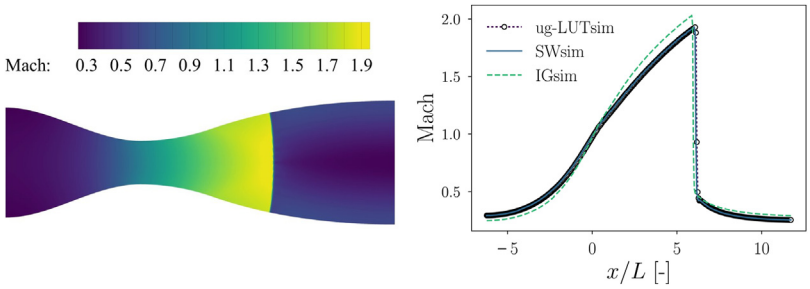

(a) Mach number contour. (b) Mach number distribution.

Fig. 5. 2D inviscid supersonic nozzle simulation results, obtained with a thermodynamic mesh of approximately 20,000 nodes. (a) Mach number contour obtained with the *ug-LUT* algorithm. (b) Mach number distribution at centerline obtained from the *IGsim*, *SWsim*, and *ug-LUTsim*.

Table 1
Input parameters for the 2D inviscid *supersonic* nozzle simulation.

Parameter	Value	Unit
Working fluid	MM	–
Total inlet temperature	530.28	K
Total-to-static pressure ratio	1.84	–
Inlet compressibility factor	0.64	–
Inlet turbulence intensity	0.05	–

Table 2
Input parameters for the 2D turbulent turbine cascade simulation.

Parameter	Value	Unit
Working fluid	MDM	–
Total inlet temperature	592.30	K
Total-to-static pressure ratio	1.26	–
Inlet compressibility factor	0.598	–

and the working fluid is siloxane MM. Table 1 reports the main simulation parameters.

In order to assess the performance of the method, the computational cost of the nozzle simulation relying on the *ug-LUT* algorithm for the evaluation of fluid properties (*ug-LUTsim*) is compared with one in which the properties are provided to the flow solver by the external thermodynamic library based on the Span-Wagner EoS (*SWsim*), for an increasing number of thermodynamic mesh nodes. Fig. 4a shows the computational cost of *ug-LUTsim* as a function of the mesh nodes, normalized with the computational cost of *SWsim*. Fig. 4b reports the root-mean-square error (RMSE) between the flow field Mach number of *ug-LUTsim* with respect to *SWsim* for different thermodynamic mesh refinements. As expected, the RMSE value decreases with the number of thermodynamic mesh elements, whereas the computational cost shows the opposite trend.

Fig. 5b shows a comparison of the Mach number calculated at the nozzle center line with *ug-LUTsim* and simulation results in which fluid properties are evaluated with the ideal-gas model (*IGsim*) and with a model based on the Span-Wagner EoS (*SWsim*). The streamwise Mach distribution obtained with *ug-LUTsim* is well in agreement with the results of *SWsim*. As expected, both deviate from the distribution obtained with *IGsim*, considering that the inlet compressibility factor significantly departs from unity ($Z = 0.64$).

3.2. Turbulent transonic 2D turbine cascade

The turbine cascade reported in Fig. 6a was simulated under transonic conditions, in order to evaluate the performance of the *ug-LUT* method in case of RANS simulations. A hybrid mesh of approximately 40,000 elements was used to discretize the computational domain, with about 15,000 quads in the proximity of the blade surface to ensure $y^+ \approx 1$. The simulation parameters are listed in Table 2. For this test case MDM is considered as working fluid.

Similarly to the previous test case, Fig. 7 reports the same trend in terms of computational cost and RMSE based on the Mach flow field. However, the computational gain provided in the RANS simulation is approximately 4 times higher as compared to the inviscid test case. Fig. 6b shows the comparison between the dimensionless static pressure, along the blade profile, from the *IGsim*, the *SWsim*, and the *ug-LUTsim*. The results achieved with the *SWsim* are well in agreement with *ug-LUTsim*, while both differ from the ones obtained with *IGsim*.

In order to further investigate the performance of the proposed tabular method, the same turbine configuration is simulated with the binary mixture MDM(85%)/MM(15%) as working fluid. For this test case, the cost reduction is approximatively 5 times higher than the computation of the single-component working fluid (Fig. 8b), while retaining the same accuracy (Fig. 6a). These results show that

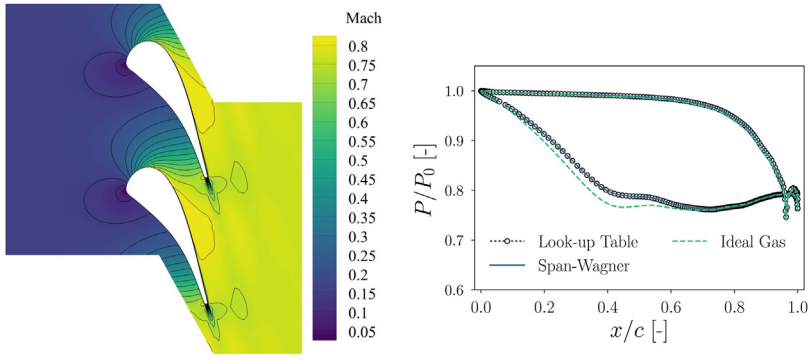

(a) Mach number contour. (b) Blade loading.

Fig. 6. 2D turbine cascade simulation results, obtained with approximately 15,000 thermodynamic mesh nodes. (a) Mach number distribution with the *ug-LUT* algorithm. (b) Blade pressure distribution obtained from the *IGsim*, *SWsim* and *ug-LUTsim*.

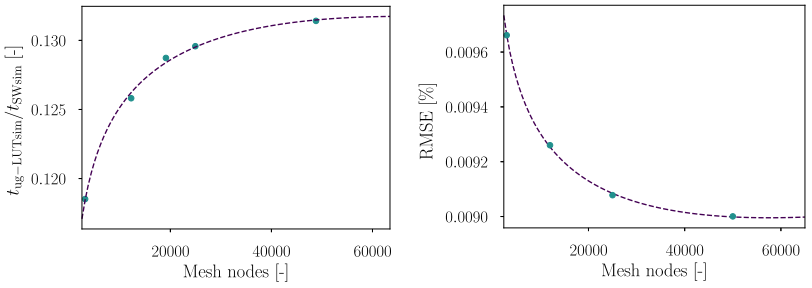

(a) Normalized computational cost. (b) RMSE error.

Fig. 7. 2D turbine cascade simulation results. (a) Normalized computational cost of the simulation employing the look-up table method (*ug-LUTsim*) compared to that of the simulation obtained using the Span-Wagner thermodynamic model (*SWsim*). (b) Relative mean square error (RMSE) of the Mach field from the *SWsim* and *ug-LUTsim*. The *SWsim* results are taken as reference.

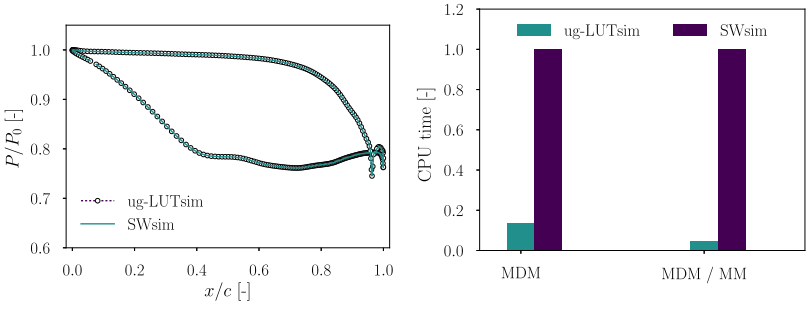

(a) Mach number contour. (b) Computational cost.

Fig. 8. 2D turbine cascade simulation results operating with the MDM(85%)/MM(15%) mixture. (a) Blade pressure distribution obtained from *ug-LUTsim* and *SWsim*. (b) Comparison between computational time associated with the single-component working fluid (MDM) and the MDM(85%)/MM(15%) mixture. Results are normalized using the computational time associated with the *SWsim*.

the use of the LuT method is even more attractive when applied to flow problems involving mixtures.

3.3. Turbulent 3D supersonic turbine cascade

The supersonic stator of the Organic Rankine Cycle turbine, documented in Ref. [27], is finally considered to investigate the computational efficiency of the unstructured-based look-up table method for three-dimensional RANS simulations. The numerical parameters of the test case are provided in Table 3. The physical mesh consists of about one million cells and thermodynamic grid is composed by approximately 20,000 nodes.

Fig. 9a shows the contour of the density gradient: a complex flow pattern of both shock-waves and fans is present in the semi-bladed region, due to the post-expansion phenomena. Fig. 9b displays the density field relative error between the *ug-LUTsim* and the *SWsim*. The deviation in the order of 0.1% points out that, even with a relatively coarse thermodynamic grid, the tabular approach is accurate for three-dimensional problems involving complex flow phenomena. Furthermore, the computational cost reduction for the 3D

Table 3
Input parameters for the 3D turbulent *ORCHID* turbine cascade simulation.

Parameter	Value	Unit
Working fluid	MM	–
Total inlet temperature	573.15	K
Total-to-static pressure ratio	14.71	–
Inlet compressibility factor	0.77	–
Inlet turbulence intensity	0.05	–

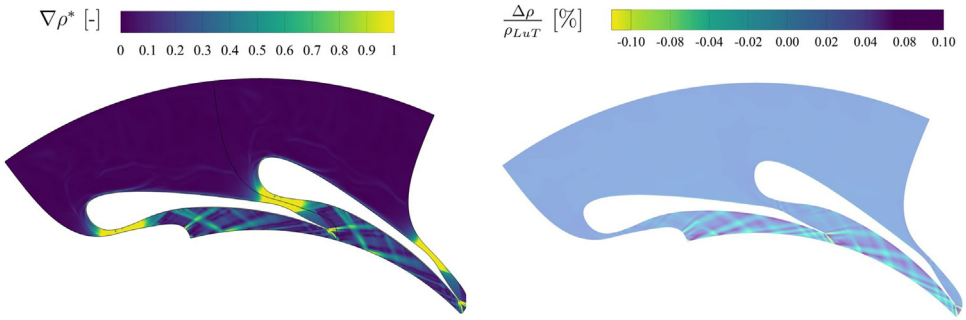

(a) Density gradient contour. (b) Density relative error.

Fig. 9. 3D turbine cascade simulation results. (a) Normalized density gradient distribution obtained with the *ug-LUT* algorithm. (b) Density relative error between the *ug-LUTsim* and the *SWsim* results, for approximately 15,000 thermodynamic mesh nodes.

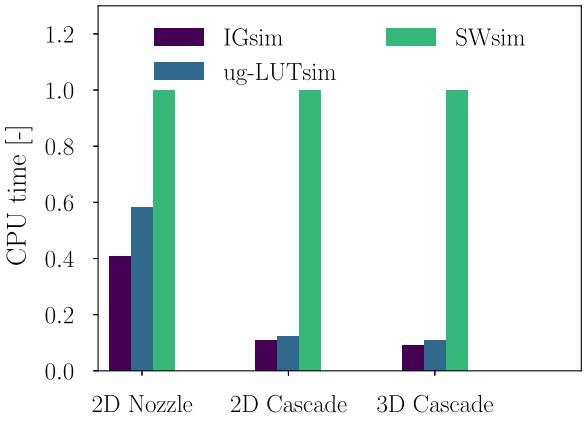

Fig. 10. Summary of the computational time for the selected test-cases. Results are normalized using the computational time associated with the *SWsim* and based on a thermodynamic mesh of approximately 15,000 nodes.

RANS simulation is very similar to the analysed 2D RANS test case, as shown in Fig. 10.

4. Performance and memory assessment

An equally spaced structured grid-based LuT method was implemented within *SU2*, in order to assess the performance of *ug-LUT*. The structured-based LuT algorithm was considered for carrying out a comparison in terms of computational cost and memory requirements because of its simple data structure and efficiency. The turbine cascade, described in Section 3.2, is selected as reference test case to perform this analysis. The nomenclature *sg-LUT* and *ug-LUT* is used hereinafter to refer to the structured-based and the unstructured-based LUT method, respectively.

4.1. *Structured-grid LuT algorithm* | sg-LUT

The structured grid LuT (*sg-LUT*) implementation features the same interpolation method of *ug-LUT*. Thermodynamic query vectors, for the CFD application considered, are: (P, T), (P, ρ), (P, s), (ρ, T), (h, s). By selecting the thermodynamic mesh as a function of pressure and density (Fig. 11), the searching algorithm is based on simple binary search for (P, T), (P, ρ), (P, s), (ρ, T), because they have at least one common input with respect to thermodynamic mesh. A *kd-tree* is used for the (h, s) pair. Fig. 11 shows an example of both structured and unstructured mesh of thermodynamic region of interest, generated using the same number of mesh nodes.

4.2. *Comparison* sg-LUT *vs.* ug-LUT

Fig. 12a and b reports the normalized CPU time associated with the *sg-LUTsim* and *ug-LUTsim*. The total time includes both the LuT pre-processing and the total CFD solver iteration time. As can be noticed (Fig. 12b), the preprocessing time becomes a relevant fraction of the total time for *ug-LUT* as opposed to *sg-LUT*. This is due to the trapezoidal map generation for each thermodynamic input pair. This operation is done just once for *sg-LUT*, when creating the *kd-tree* relative to the (h, s) input pair.

The ratio between the total simulation time obtained by *ug-LUT* and *sg-LUT* (Fig. 13a) indicates that *ug-LUT* is faster than *sg-LUT*, for thermodynamic meshes that are approximately composed by a number of mesh nodes lower than 10,000. The *sg-LUT* is about 5% faster than *ug-LUT* for 25,000 thermodynamic mesh nodes. The *ug-LUT* performance is in agreement with the computational cost of LuT based on quad-tree data structures, whose computational cost has been found to be 10% higher than equally spaced structured tabulation methods [13]. Fig. 13b shows the comparison between the memory requirements of *ug-LUT* and *sg-LUT*. The *ug-LUT* memory

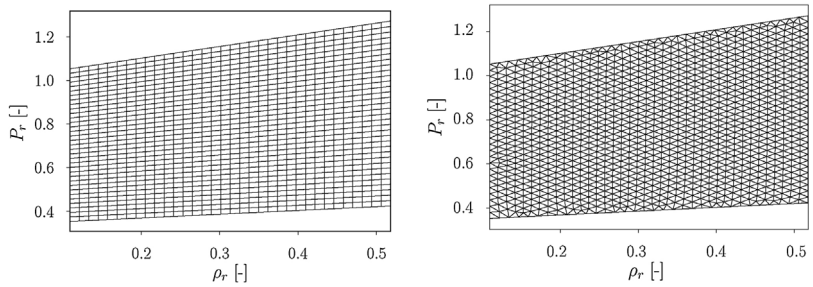

(a) Structured mesh. (b) Unstructured mesh.

Fig. 11. Mesh of thermodynamic region of interest for the turbine cascade test case, as a function of the reduced density ρ_r and reduced pressure P_r. (a) Example of structured mesh used for *sg-LUT*. (b) Example of unstructured mesh used for *ug-LUT*.

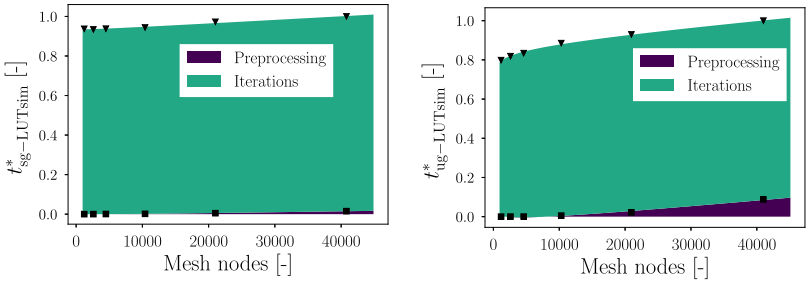

(a) *sg-LUT* CPU Time. (b) *ug-LUT* CPU time.

Fig. 12. Normalized pre-processing and CFD iterations computational time t^* as a function of thermodynamic mesh nodes. The maximum total CPU time relative to each algorithm is used as reference value. (a) Computational time of the *sg-LUT* algorithm. (b) Computational time of the *ug-LUT* algorithm.

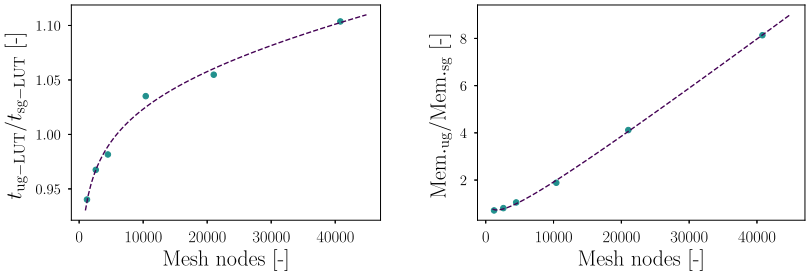

(a) CPU time ratio. (b) Memory ratio.

Fig. 13. Total CPU time and memory ratio between *ug-LUT* and *sg-LUT*. (a) Computational time ratio. (b) Memory requirements ratio.

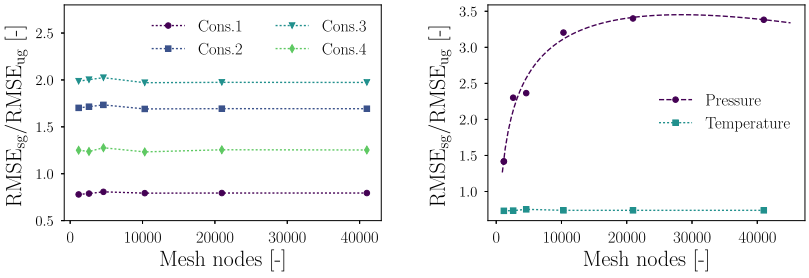

(a) Conservative Variables. (b) Pressure and Temperature.

Fig. 14. Relative mean square error ratio between *sg-LUT* and *ug-LUT*. (a) RMSE ratio of the conservative variables. (b) RMSE ratio of pressure and temperature.

requirements are higher than *sg-LUT* mainly due to the following reasons: (i) in *ug-LUT* the trapezodial maps are created for all thermodynamic input pairs; (ii) for *ug-LUT* the unstructured-mesh connectivity has to be stored. For practical applications, however, since thermodynamic meshes featuring around 10,000 elements are deemed sufficient for the required level of accuracy, the absolute memory associated never exceeded 200 Mb. Furthermore, for problems discretized on large domains both the preprocessing computational cost and the memory burden are expected to be a negligible fraction when compared with the CPU time and memory requirements of the CFD simulation.

Finally, a comparative assessment of the RMSE with respect to the *SWsim* is carried out for both *ug-LUT* and *sg-LUT*. Fig. 14 depicts the ratio between the RMSE obtained by *ug-LUT* and *sg-LUT* relative to the conservative variables ρ, ρv_1, ρv_2, ρe (Fig. 14a), pressure and temperature (Fig. 14b). The RMSE is calculated, as shown in Section 3, with respect to *SWsim*. The *ug-LUT* algorithm is more accurate than *sg-LUT*, for the fluxes ρv_1, ρv_2, ρe, and the pressure while the opposite occurs with regard to the density and temperature. Without being exhaustive, these results indicate that unstructured tabular methods may be advantageous when it comes to accuracy as compared to structured grids characterized by the same number of nodes and level of refinement.

5. Conclusions

This paper documents the *ug-LUT* method, a novel look-up table method that can be used to improve the computational performance in non-ideal compressible fluid dynamics (NICFD) simulations. The method is based on an unstructured mesh in combination with a trapezoidal-map searching algorithm and a piece-wise interpolation method based on the duality approach. The algorithm was successfully implemented in the open-source code SU2 and its performance assessed in three paradigmatic NICFD cases: (1) an inviscid 2D supersonic nozzle; (2) a 2D RANS transonic turbine cascade; (3) a 3D RANS supersonic stator row. In all cases, thermodynamic property model of reference is based on a multi-parameter technical equation of state.

The outcome of this study can be summarized as follows:

- The *ug-LUT* method provides a computational cost reduction compared to simulations in which properties are calculated

directly by means of an external fluid property library of approximately one order of magnitude for RANS computations, whereas it is twice less expensive in case of inviscid simulations.
- The accuracy level was found to be satisfactory ($RMSE < 0.01\%$) for engineering applications, with a simple linear interpolation and a relatively coarse thermodynamic grid (of the order of 15,000 elements).
- The method is very efficient for flow simulations involving mixtures as working fluids, for which direct calculation of fluid properties might be prohibitive. The relative computational gain, for the analyzed test case, is five times higher if compared to simulations involving pure fluids.
- *ug-LUT* can be regarded as an alternative algorithm to structured LuT methods, providing the possibility of using mesh refinement and featuring comparable performance and accuracy.

Current work is focused on extending the *ug-LUT* method to enable automatic differentiation of the LuT for adjoint-based shape optimization of NICFD problems and to allow its use in other demanding simulations, like dynamic system simulations of energy conversion systems.

Acknowledgements

This research has been supported by Robert Bosch GmbH and the Applied and Engineering Sciences Domain (TTW) of the Dutch Organization for Scientific Research (NWO), Technology Program of the Ministry of Economic Affairs, grant number 13385.

Appendix A.

Here, the pseudo-codes of the algorithms used for the Trapezoidal Map presented in Sec. 2.2 are reported.

Algorithm 1. Build Trapezoidal Map **is**.

1: **input:** list of unique edges: *Edges*;
2: list of edge to face connectivities: *EdgeToFace*;
3: list of the x-coordinates of the edges: $x_{samples}$;
4: list of the y-coordinates of the edges: $y_{samples}$;
5: **output:** list of unique x bands through which to search: X_{Bands};
6: list of connectivity of edges to a given unique x-band (order by y-value of edge at middle of band): $Y_{WithinBands}$;
7: Filter out vertical edges from $X_{samples}$ creating unique list: x_{Bands};
8: **for** each band b in X_{Bands} **do**
9: **for** each edge e in Edges **do**
10: **if** e intersects b then Add e to $Y_{WithinBands}$
11: **end if**
12: **end for**
13: Sort the edges in $Y_{WithinBands}$ according to the y value of the edge in the center of the band
14: **end for**
15: **return:** X_{Bands}, $Y_{WithinBands}$;

Algorithm 2. Trapezoidal Map **is**.

1: **input:** 2D query point (what to search for): x, y;
2: list of edge to face connectivities: *EdgeToFace*;
3: list of unique x bands through which to search: X_{Bands};
4: list of connectivity of edges to a given unique x-band (ordered by y-value of edge at middle of band): $Y_{WithinBands}$;
5: **output:** the index of the face in which the query point lies: *CF*;
6:
7: Use binary search to find band b in X_{Bands} which contains x;
8: Within band b use a binary search to find edge e_1 (below the query point) and e_2 (above the query point);
9: Use interpolation to check if edge is below or above the query point;
10: The containing face CF is given by the intersection of the edge to face connectivities of e_1 and e_2;
11: **return**: *CF*;

References

[1] P. Colonna, E. Casati, C. Trapp, T. Mathijssen, J. Larjola, T. Turunen-Saaresti, A. Uusitalo, Organic rankine cycle power systems: from the concept to current technology, applications, and an outlook to the future, J. Eng. Gas Turbines Power 137 (10) (2015) 100801.
[2] Y. Kim, C. Kim, D. Favrat, Transcritical or supercritical CO_2 cycles using both low- and high-temperature heat sources, Energy 43 (1) (2012) 402–415.
[3] J. Ahamed, R. Saidur, H. Masjuki, A review on exergy analysis of vapor compression refrigeration system, Renew. Sustain. Energy Rev. 15 (3) (2011) 1593–1600.
[4] B.P. Brown, B.M. Argrow, Application of Bethe–Zel'dovich–Thompson fluids in organic Rankine cycle engines, J. Propuls. Power 16 (6) (2000) 1118–1124.
[5] P. Colonna, N. Nannan, A. Guardone, T. Van der Stelt, On the computation of the fundamental derivative of gas dynamics using equations of state, Fluid Phase Equilib. 286 (1) (2009) 43–54.
[6] G. Gori, 1st International Seminar on Non-Ideal Compressible-Fluid Dynamics for Propulsion & Power, 821(1, 2017, pp. 011001.
[7] S. Bahamonde, M. Pini, C. De Servi, A. Rubino, P. Colonna, Method for the preliminary fluid dynamic design of high-temperature mini-organic rankine cycle turbines, J. Eng. Gas Turbines Power 139 (8) (2017) 082606.
[8] M. Pini, G. Persico, D. Pasquale, S. Rebay, Adjoint method for shape optimization in real-gas flow applications, J. Eng. Gas Turbines Power 137 (3) (2015) 032604.
[9] M. Pini, A. Spinelli, G. Persico, S. Rebay, Consistent look-up table interpolation method for real-gas flow simulations, Comput. Fluids 107 (2015) 178–188.
[10] P. Boncinelli, F. Rubechini, A. Arnone, M. Cecconi, C. Cortese, Real gas effects in turbomachinery flows: a computational fluid dynamics model for fast computations, J. Turbomach. 126 (2) (2004) 268–276.
[11] M. Dumbser, U. Iben, C.D. Munz, Efficient implementation of high order unstructured WENO schemes for cavitating flows, Comput. Fluids 86 (2013) 141–168.
[12] M. De Lorenzo, P. Lafon, M. Di Matteo, M. Pelanti, J.-M. Seynhaeve, Y. Bartosiewicz, Homogeneous two-phase flow models and accurate steam-water table look-up method for fast transient simulations, Int. J. Multiph. Flow. (2017).
[13] G. Xia, D. Li, C.L. Merkle, Consistent properties reconstruction on adaptive cartesian meshes for complex fluids computations, J. Comput. Phys. 225 (1) (2007) 1175–1197.
[14] Ø. Wilhelmsen, A. Aasen, G. Skaugen, P. Aursand, A. Austegard, E. Aursand, M.A. Gjennestad, H. Lund, G. Linga, M. Hammer, Thermodynamic modeling with equations of state: present challenges with established methods, Ind. Eng. Chem. Res. 56 (13) (2017) 3503–3515.
[15] K. Yiu, D. Greaves, S. Cruz, A. Saalehi, A. Borthwick, Quadtree grid generation: information handling, boundary fitting and CFD applications, Comput. Fluids 25 (8) (1996) 759–769.
[16] F. Palacios, J. Alonso, K. Duraisamy, M. Colonno, J. Hicken, A. Aranake, A. Campos, S. Copeland, T. Economon, A. Lonkar, et al., Stanford University Unstructured (SU2): an open-source integrated computational environment for multi-physics simulation and design, 51st AIAA Aerospace Sciences Meeting Including the New Horizons Forum and Aerospace Exposition (2013) 287.
[17] T.D. Economon, F. Palacios, S.R. Copeland, T.W. Lukaczyk, J.J. Alonso, SU2: an open-source suite for multiphysics simulation and design, AIAA J. 54 (3) (2015) 828–846.
[18] M. Pini, S. Vitale, P. Colonna, G. Gori, A. Guardone, T. Economon, J. Alonso, F. Palacios, SU2: the open-source software for non-ideal compressible flows, J. Phys. Conf. Ser. 821 (2017) 012013.
[19] A. Ghidoni, E. Pelizzari, S. Rebay, V. Selmin, 3D anisotropic unstructured grid generation, Int. J. Numer. Methods Fluids 51 (9-10) (2006) 1097–1115.
[20] P. Colonna, T. Van der Stelt, Fluidprop: A Program for the Estimation of Thermo Physical Properties of Fluids, Energy Technology Section, Delft University of Technology, Delft, The Netherlands, 2018, http://www.FluidProp.com.
[21] P. Colonna, N. Nannan, A. Guardone, E.W. Lemmon, Multiparameter equations of state for selected siloxanes, Fluid Phase Equilib. 244 (2) (2006) 193–211.
[22] M. De Berg, M. Van Kreveld, M. Overmars, O.C. Schwarzkopf, Computational Geometry, Springer, 2000, pp. 1–17.
[23] M.B. Giles, N.A. Pierce, An introduction to the adjoint approach to design, Flow Turbulence Combust. 65 (3) (2000) 393–415.
[24] S. Vitale, G. Gori, M. Pini, A. Guardone, T.D. Economon, F. Palacios, J.J. Alonso, P. Colonna, Extension of the SU2 open source CFD code to the simulation of turbulent flows of fluids modelled with complex thermophysical laws, 22nd AIAA Computational Fluid Dynamics Conference (2015) 2760.
[25] M. Vinokur, J.-L. Montagné, Generalized flux-vector splitting and roe average for an equilibrium real gas, J. Comput. Phys. 89 (2) (1990) 276–300.
[26] B. Van Leer, Towards the ultimate conservative difference scheme. v. a second-order sequel to Godunov's method, J. Comput. Phys. 32 (1) (1979) 101–136.
[27] M. Pini, C. De Servi, M. Burigana, S. Bahamonde, A. Rubino, S. Vitale, P. Colonna, Fluid-dynamic design and characterization of a mini-orc turbine for laboratory experiments, Energy Proc. 129 (2017) 1141–1148.